catalysts

MDPI

*Article*

# Heterogeneous Photocatalytic Oxidation and Detoxification of Simulated Agricultural Wastewater Contaminated with Boscalid Fungicide Using g-$C_3N_4$ Catalyst

**Maria Antonopoulou [1,*], Anna Tzamaria [1], Kleopatra Miserli [2], Christos Lykos [2] and Ioannis Konstantinou [2,3]**

[1] Department of Sustainable Agriculture, University of Patras, GR-30131 Agrinio, Greece; annatz408@gmail.com
[2] Department of Chemistry, University of Ioannina, GR-45110 Ioannina, Greece; miserlikleo@gmail.com (K.M.); c.lykos93@gmail.com (C.L.); iokonst@uoi.gr (I.K.)
[3] Institute of Environment and Sustainable Development, University Research and Innovation Center, GR-45110 Ioannina, Greece
* Correspondence: mantonop@upatras.gr; Tel.: +30-26410-74114

**Abstract:** In the present study, the photocatalytic oxidation and detoxification of aqueous matrices contaminated with boscalid using g-$C_3N_4$ catalyst and UV-A light was investigated. The UV-A/g-$C_3N_4$ process was found to achieve higher than 83% removal of boscalid in both matrices, with $h^+$ and $O_2^{\bullet-}$ being the main species. UHPLC-HRMS analysis allowed the identification of five TPs, while the main degradation pathways involved hydroxylation, cyclization, and dechlorination. *Scenedesmus rubescens* microalgae species was exposed to boscalid solutions and lake water spiked with the fungicide before the photocatalytic treatment and inhibition in the growth rate was observed. An increase in the toxicity was also observed during the first stages of the treatment. The results from the in silico study correlate with the observed evolution of ecotoxicity during the application of the process, as some of the identified TPs were found to be toxic or very toxic for aquatic organisms. However, prolonged application of the process can lead to detoxification. It was also observed that the g-$C_3N_4$ catalyst can retain its photochemical stability and activity after at least three cycles. However, a slight decrease in the activity was observed when repeated another two times. This study demonstrated that the suggested photocatalytic process can both decrease the harmful effects of boscalid as well as effectively lower its concentration in water.

**Keywords:** g-$C_3N_4$ catalyst; boscalid; degradation; detoxification; transformation products; reusability



**Citation:** Antonopoulou, M.; Tzamaria, A.; Miserli, K.; Lykos, C.; Konstantinou, I. Heterogeneous Photocatalytic Oxidation and Detoxification of Simulated Agricultural Wastewater Contaminated with Boscalid Fungicide Using g-$C_3N_4$ Catalyst. *Catalysts* **2024**, *14*, 112. https://doi.org/10.3390/catal14020112

Academic Editor: Omid Akhavan

Received: 30 December 2023
Revised: 22 January 2024
Accepted: 26 January 2024
Published: 31 January 2024



## 1. Introduction

Heterogeneous photocatalysis is one of the most well-studied advanced oxidation processes (AOPs). Numerous studies have been conducted in the last thirty years that have proved its efficiency for the removal of different contaminants from water and wastewater [1]. The first studies focused mainly on the efficiency of the process using different semiconducting inorganic oxides such as $TiO_2$ and ZnO [2]. The high efficiency of this process to remove organic contaminants and heavy metals from aqueous matrices led to the investigation of alternative catalysts with the aim to overcome some limitations [3].

In recent years, graphitic carbon nitride (g-$C_3N_4$) possessing a layered structure similar to graphite has become a promising organic semiconductor with high photocatalytic activity in visible light (bandgap of ~2.7 eV). It has been used for various environmental applications, such as water and wastewater treatment, $CO_2$ and NOx reduction, and hydrogen production, amongst others, due to its interesting and unique physicochemical properties such as good chemical and thermal stability [4–13]. In addition, compared with other photocatalysts, g-$C_3N_4$ can be easily synthesized by various synthesis techniques using melamine, cyanamide, urea, thiourea, and ammonium thiocyanate as raw materials [14,15].

The rapid increase in industrialization and the population explosion have led to water pollution as various contaminants are introduced into the aquatic environment by different sources. The worry over chemical contamination of water is a significant issue in the twenty-first century [6,16]. Recently, various categories of pollutants have been found in water, such as metal ions, personal care products, pharmaceuticals, pesticides, and dyes, among others. The presence of these pollutants in the aquatic systems poses a threat to ecosystems and humans [6,16].

Pesticide contamination has raised great concern worldwide, and pesticide residues can be found in soil and aquatic systems, exerting detrimental effects on the environment and human health [17,18]. Boscalid [2-chloro-N(4′-chloro-biphenyl-2-yl)-nicotinamide] is a carboxamide fungicide used against fungal plant diseases in agriculture. Following its application, excessive amounts of this fungicide can be adsorbed on soil particles or/and introduced into aquatic systems [18]. It has been widely found in a variety of environmental compartments and is thought to be persistent. Through spray drift, leaching, and runoff following its application, boscalid can penetrate the soil and reach surface- and ground-waters, with dissipation half-lives (DT50) in the range of 322 to 365 days [19]. Boscalid has also been characterized as a moderate leacher and consequently can pollute surface- and ground-water [20].

Boscalid has been detected at a frequency of 72% in the USA in surface- and ground-waters [18], and in the coastal watersheds of California, USA, it has been detected at concentrations of up to 36 μg $L^{-1}$ [21]. Moreover, it has been detected in fish and crab samples collected from the Californian estuary [22]. The long-term accumulation of boscalid in water can have various negative effects on aquatic organisms. For instance, it is toxic to zebrafish embryos [23] and presents various effects in *Daphnia magna* [24], microalgae such as *Chlorella vulgaris* [25], and the amphipod *Gammarus fossarum* [26].

Thus, its effective removal from aqueous phases has attracted scientific interest. Among different AOPs, heterogeneous photocatalysis has been evaluated for the removal of boscalid from aqueous matrices using mainly $TiO_2$-based and ZnO catalysts [27–32]. Despite significant advancements in photocatalysis research in recent years, the effectiveness of this process in the removal of boscalid using alternative photocatalysts remains limited. Additionally, previous investigations utilizing g-$C_3N_4$ have primarily been conducted in controlled laboratory aqueous matrices rather than environmental matrices [33]. Notably, there is a dearth of scientific literature reporting on the degradation of boscalid in water using g-$C_3N_4$ catalysts, especially when combined with biological techniques to assess the toxicity.

Ambiguously, the development of visible light-active photocatalysts holds promise for leveraging renewable energy resources, potentially reducing energy consumption and overall costs. Consequently, in the present study the photocatalytic oxidation and detoxification of aqueous matrices contaminated with boscalid was investigated using g-$C_3N_4$ and UV-A irradiation (mainly 365 nm). The photocatalytic process was first evaluated in terms of its effectiveness to remove boscalid from ultrapure water (UPW) and lake water (LW) contaminated with the fungicide. In the second approach, the process efficiency was assessed by investigating the ecotoxicity potency of the treated solutions through the microalgae *Scenedesmus rubescens*. Efforts were also directed toward the identification of the main transformation products (TPs) using ultra-high-performance liquid chromatography coupled with high resolution mass spectrometry (UHPLC/HRMS). The ecotoxicity of boscalid and its tentatively identified TPs as well as assessments of the important toxicological factors (e.g., mutagenicity) of these compounds were performed using three different publicly available in silico tools.

## 2. Results and Discussion

### *2.1. Photocatalytic Degradation Performance*

Before the evaluation of the performance of the UV-A/g-$C_3N_4$ process to degrade boscalid from the water, control experiments were conducted. The results from the adsorp-

tion and photolysis experiments, as depicted in Figure 1, prove that both processes cannot significantly remove the studied contaminant under the adopted experimental conditions.

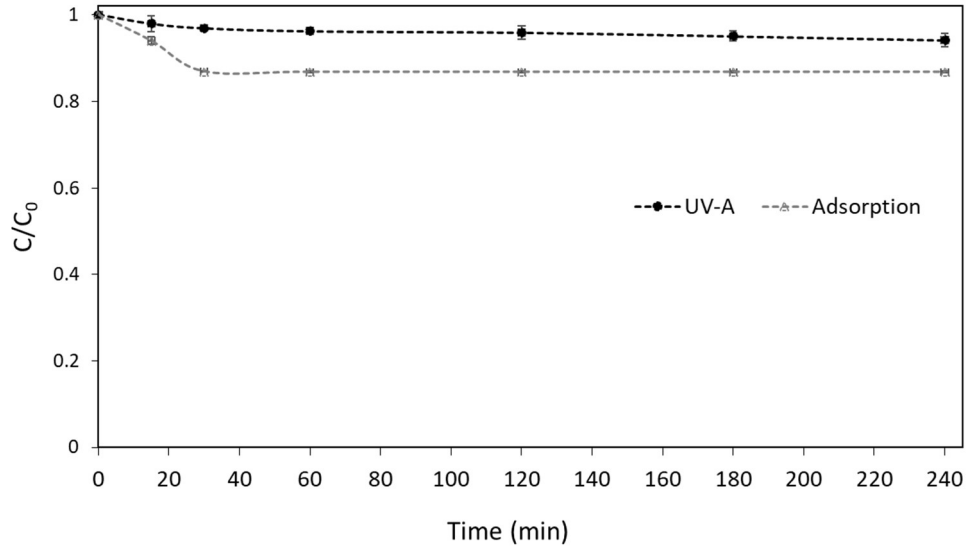


**Figure 1.** Control Experiments of boscalid in UPW ([Boscalid]$_0$ = 1 mg L$^{-1}$, [g-$C_3N_4$] = 400 mg L$^{-1}$).

In contrast, the UV-A/g-$C_3N_4$ process was found to achieve higher than 83% removal of boscalid in both matrices (UPW and LW), as depicted in Figure 2. The observed efficiency can be correlated with the good characteristics of the used g-$C_3N_4$ photocatalyst (BET SSA = 35 m$^2$ g$^{-1}$, particle size of 25 nm, Eg = ~2.82 eV), which was synthesized and characterized in a previous work [34]. The g-$C_3N_4$ photocatalyst (2.82 eV) [34] can be activated by UV-A light generating $h^+/e^-$ pairs (Equation (1)), which can initiate various reactions according to Equations (2)–(5) [15,35,36]:

$$g - C_3N_4 + hv \rightarrow h^+ + e^- \quad (1)$$

$$O_2 + e^- \rightarrow O_2^{\bullet -} \quad (2)$$

$$O_2^{\bullet -} + H^+ \rightarrow HO_2^{\bullet} \quad (3)$$

$$2\,HO_2^{\bullet} \rightarrow O_2 + H_2O_2 \quad (4)$$

$$H_2O_2 + O_2^{\bullet -} \rightarrow HO^{\bullet} + OH^- + O_2 \quad (5)$$

Similar to our results, Liu et al. (2021) [33] reports good photocatalytic activity of urea-derived carbon nitride to remove boscalid and other fungicides, under visible light irradiation. More specifically, approximately 90% boscalid (initial concentration=2 mg L$^{-1}$) removal was observed after 2 h using 500 mg L$^{-1}$ of the catalyst. In contrast, heterogeneous photocatalysis was not found to be effective for the degradation of hexaconazole using urea-derived carbon nitride (15%) [33]. The photocatalytic degradation of atrazine herbicide by g-$C_3N_4$ (prepared via pyrolysis of urea) was 52.57% after 60 min of visible light irradiation [37]. A slower degradation rate was also reported by Altendji and Hamoudi (2023) [38]. Visible light photocatalysis using g-$C_3N_4$, synthesized via urea pyrolysis, led to only 40% removal of atrazine after 5 h [38].

The experimental data were fitted in pseudo-first order reaction kinetics [4,39] according to Equation (6), and the apparent rate constants, half-lives, and correlation coefficients of boscalid degradation in both matrices are reported in Table 1.

$$\frac{d[C]}{dt} = -k_{app}[\text{Boscalid}] \rightarrow \frac{[C]}{[C]_o} = e^{-k_{app}t} \rightarrow \ln\frac{[C]}{[C]_o} = -k_{app}t \quad (6)$$

An apparent degradation constant ($k_{app}$) equal to $9.0 \times 10^{-3}$ $min^{-1}$ and a half-life of $t_{1/2}$ = 77.0 min were calculated in UPW. A lower degradation rate was observed in LW ($k = 7.2 \times 10^{-3}$ $min^{-1}$ and $t_{1/2}$ = 96.3 min).

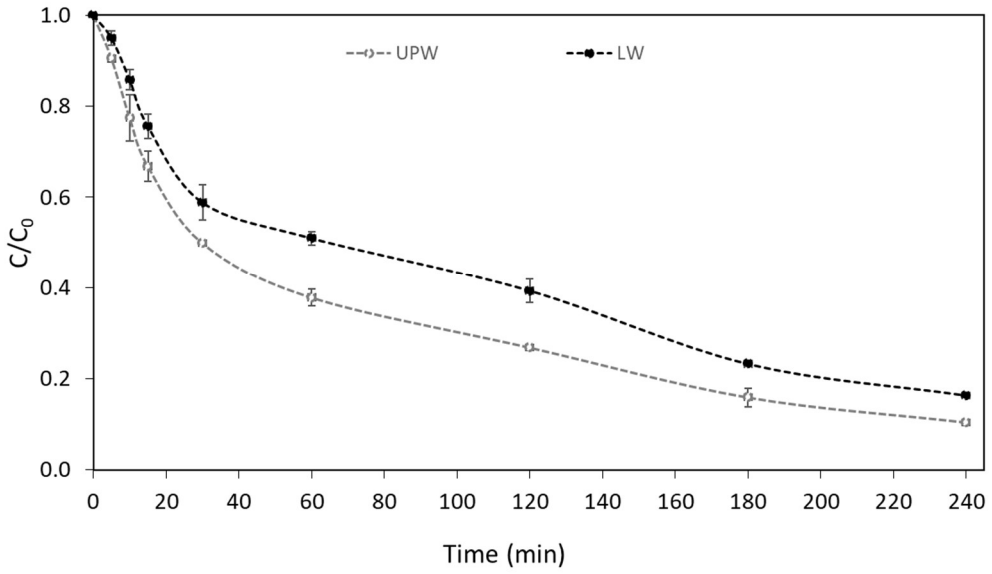


**Figure 2.** Photocatalytic degradation of boscalid in UPW and LW ([Boscalid]$_0$ = 1 mg $L^{-1}$, [g-$C_3N_4$] = 400 mg $L^{-1}$).

The chemical composition of LW and the coexistence of inorganic and organic chemicals that can compete with boscalid for the produced reactive species can be linked to the reduced degradation rate observed in LW [40]. Furthermore, some of the substances in LW have the ability to be absorbed by the g-$C_3N_4$ photocatalyst, changing or blocking its active sites [40,41]. Nonetheless, significant degradation percentages were attained in LW, demonstrating the effectiveness of this process through the emergence of reactive species.

**Table 1.** Apparent rate constants ($k_{app}$), half-lives ($t_{1/2}$), and correlation coefficients ($R^2$) of boscalid photocatalytic degradation in UPW and WW.

| Matrix | $k_{app}$ ($min^{-1}$) | $t_{1/2}$ (min) | $R^2$ |
|---|---|---|---|
| UPW | $9.0 \times 10^{-3}$ | 77.0 | 0.9200 |
| LW | $7.2 \times 10^{-3}$ | 96.3 | 0.9437 |

The contribution of the reactive species was further confirmed by scavenging experiments (Figure 3). The addition of KI provoked a strong inhibition, highlighting the significant role of $h^+$ in the degradation. The significant role of $O_2^{\bullet-}$ was confirmed when a deoxygenated experiment was conducted under $N_2$ atmosphere, as its generation requires adsorbed oxygen on the catalyst surface [15]. The tertiary alcohol t-BuOH was used as an efficient scavenger for $HO^{\bullet}$ as its reaction rate with $HO^{\bullet}$ has been reported to be in the range of 3.8–7.6 $\times$ $10^8$ $M^{-1}s^{-1}$ [42] but based on the observed inhibition $HO^{\bullet}$ contributes only slightly to the degradation of boscalid. The results are consistent with previous studies [35,36,43] that reported that the same species ($h^+$ and $O_2^{\bullet-}$) contribute significantly to the degradation of organic pollutants using g-$C_3N_4$-based heterogeneous photocatalysis.

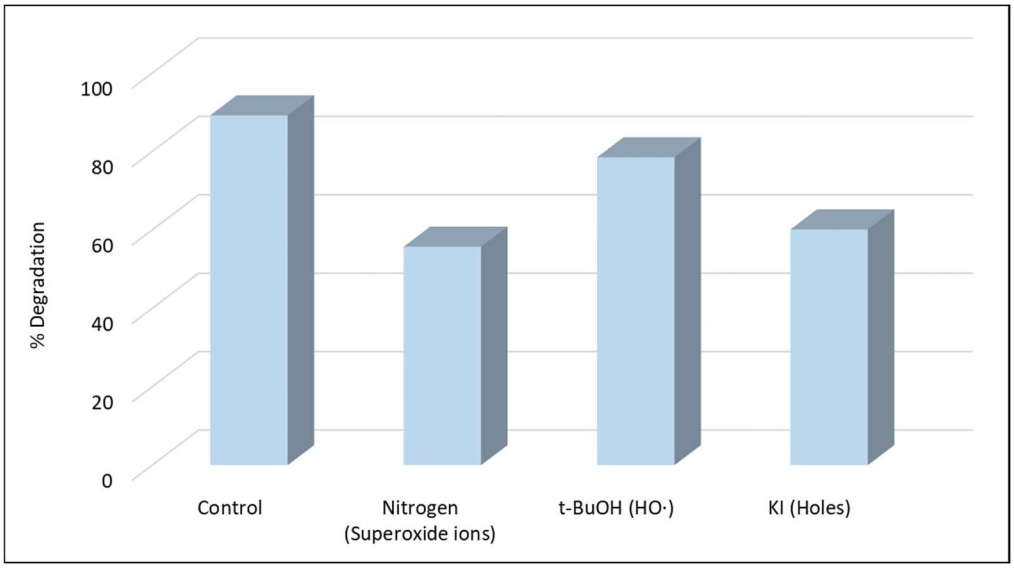


**Figure 3.** Photocatalytic degradation of boscalid in the presence of scavengers ([Boscalid]$_0$ = 1 mg $L^{-1}$, [g-$C_3N_4$] = 400 mg $L^{-1}$, [t-BuOH] = 0.1 mol $L^{-1}$, [KI] = 0.1 mol $L^{-1}$).

As it is well known, the $e^-$ in the valence band (VB) of the g-$C_3N_4$ catalyst is excited to its conduction band (CB) after the absorption of photons with energy ≥ to its energy gap (Eg), with the simultaneous generation of $h^+$ in the VB (Equation (1)). Moreover, the $e^-$ can react with absorbed $O_2$ on the surface of g-$C_3N_4$ and generate $O_2^{\bullet-}$ as the redox potential of $O_2^{\bullet-}/O_2$ (−0.13 eV vs. NHE) is much higher than that of the $E_{CB}$ (−1.3 eV) of g-$C_3N_4$ (Equation (2)) [15]. In contrast, in g-$C_3N_4$ heterogeneous photocatalysis the formation of $HO^\bullet$ cannot take place through the direct water or $OH^-$ oxidation by holes as the VB edges of the catalyst are less positive (+1.40 eV vs. NHE) than the redox potential of $OH^-/HO^\bullet$ (+1.99 eV vs. NHE) [15,36]. $HO^\bullet$ can be formed through an indirect pathway, as depicted in Equation (5).

### *2.2. Transformation Products and Pathways of Boscalid Photocatalytic Degradation*

The identified transformation products (TPs) of boscalid by photocatalytic degradation with g-$C_3N_4$ in ultrapure water (UPW) and lake water (LW) are summarized in Table S1. Analysis under negative electrospray ionization mode did not allow the identification of TPs. In positive ionization mode, boscalid presented pseudo-molecular ions at m/z 343.0397 $[M + H]^+$ (base peak) and 365.0216 $[M + Na]^+$ with the molecular formula $C_{18}H_{13}N_2OCl_2$ and $C_{18}H_{12}N_2OCl_2Na$, respectively, while $MS^2$ and $MS^3$ fragments are analogous to the assignment reported elsewhere [31,44,45]. The MS spectrum of boscalid also showed pseudo-molecular ions at *m*/*z* 345.0367 and 347.0338, corresponding to the isotopic profile of a compound containing two chlorine atoms with peak heights in the ratio of 9:6:1.

All the identified TPs revealed a smaller retention time than boscalid, denoting the more polar character. Firstly, TP_307 provided a peak at m/z 307.0628 $[M + H]^+$ with a molecular formula of $C_{18}H_{12}N_2OCl$, corresponding to $[M-36]^+$ ion generated due to the loss of HCl from molecular ion. The second TP identified (TP_325) at *m*/*z* 325.0264 with ion formula $C_{18}H_{11}N_2Cl_2$ corresponds to that of boscalid minus 18 a.m.u., suggesting water elimination from the latter. The losses of HCl and $H_2O$ suggest subsequent cyclization, which provides a more stable cation including an additional six-centered ring in which the charge is well delocalized on three sites. Positive holes ($h^+$) generated by g-$C_3N_4$ can react with the electron-rich parts of the boscalid compound by electron transfer, resulting in the formation of TP_307 and TP_325. The significant role of $h^+$ was also verified by the scavenging experiments mentioned above. Cyclized compounds TP_325 and TP_307 have also been reported in a previous study devoted to the photolytic degradation of boscalid [46].

TP_309, a degradation product with $[M+H]^+$ at $m/z$ 309.0795 and suggested formula $C_{18}H_{14}N_2OCl$, was rationalized to a dechlorinated product after the detachment of chlorine from the pyridine ring of boscalid in accordance with the previously identified compound after the biodegradation of boscalid [47]. Moreover, TP_289 presented a molecular formula $C_{18}H_{13}N_2O_2$ according to the molecular ion at $m/z$ 289.0974 $[M + H]^+$ and can be rationalized to that of TP_307 ($C_{18}H_{12}N_2OCl$) with a substitution of chlorine by the hydroxyl group. The degradation process also comprises the addition of the hydroxyl group onto one of the three available aromatic rings, TP_359, presenting a peak at $m/z$ 359.0369 with the molecular formula $C_{18}H_{13}N_2O_2Cl_2$. However, the exact site of the hydroxylation cannot be proposed. This hydroxylation pathway has also been identified by other researchers in photocatalysis by nitrogen-doped/undoped $TiO_2$ and persulfate ions [32]. A possible reaction network for boscalid degradation is shown in Figure 4. Based on the areas determined in the analysis, TP_307 was the most abundant in both UPW and LW. The other TPs showed quite similar areas. Moreover, most of the TPs started to be formed at 15 min and attained their maximum between 30 and 60 min in UPW and LW, accordingly. Thereafter, a progressive decrease in their areas was observed.

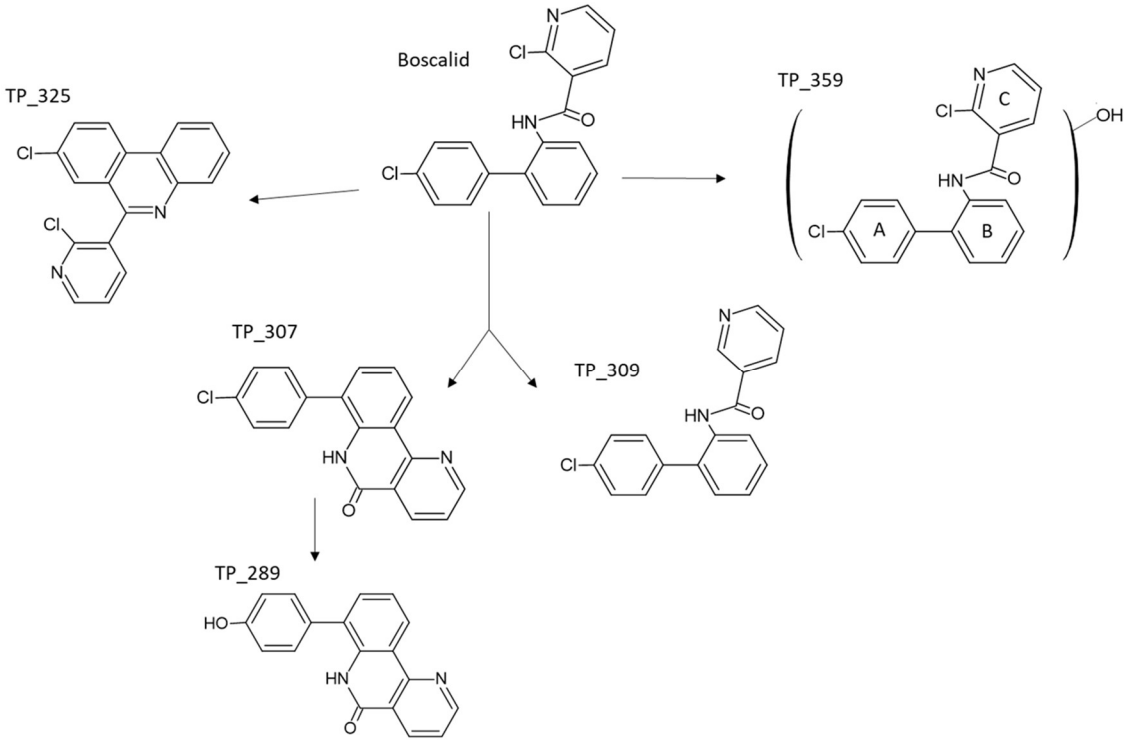


**Figure 4.** Proposed photocatalytic degradation pathways of boscalid.

### *2.3. Photocatalytic Detoxification Performance*

The evaluation of toxicity during the application of AOPs is a very important issue that needs investigation. The importance of toxicity evaluation is related with the potential formation of toxic TPs. Various aquatic microorganisms are used as bioindicators in different ecotoxicity tests. Algae are the base of the aquatic food chain, and potential detrimental effects to them can significantly affect the higher trophic levels [48]. Among the freshwater microalgae, *Scenedesmus rubescens* has been widely used in ecotoxicology studies [49,50]. The evolution of toxicity during the photocatalytic process against freshwater microalgae *Scenedesmus rubescens* was evaluated in UPW and LW (Figure 5a,b). The microalgae were exposed to untreated and treated solutions for 24, 48, and 72 h.

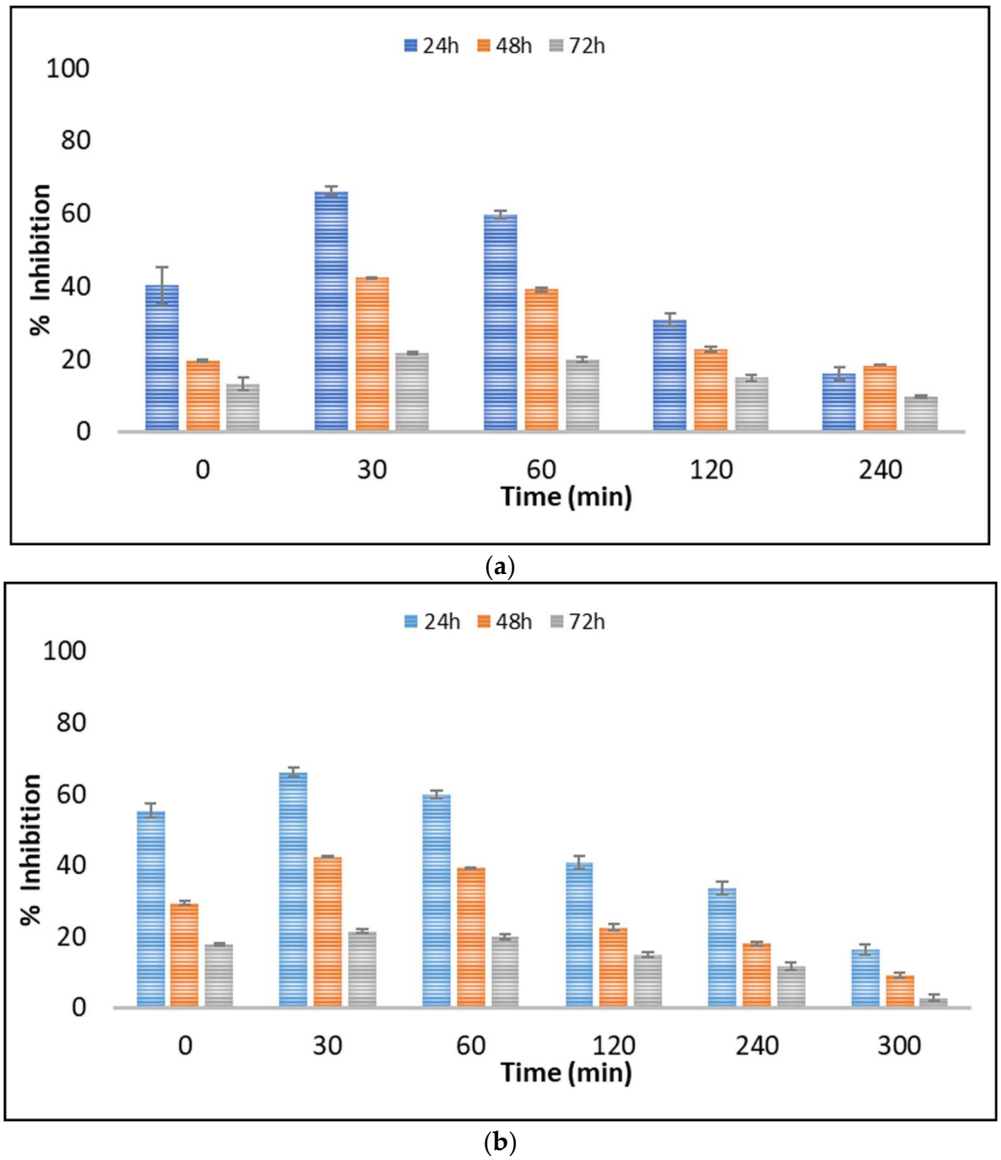


**Figure 5.** Toxicity evolution during the UV-A/g-$C_3N_4$ process in (**a**) UPW and (**b**) LW using *Scenedesmus rubescens*.

Control tests (UPW–g-$C_3N_4$ irradiated solutions, LW–g-$C_3N_4$ irradiated solutions) were also performed and showed a negligible to slight toxicity (~4–14% of inhibition) to *Scenedesmus rubescens* after 24, 48, and 72 h. Thus, concerns regarding the toxicity of nanoparticles can be excluded. The LW water was also found to provoke approximately 13.2% inhibition. According to the results depicted in Figure 5, a significant effect of 5% *v*/*v* untreated solutions of boscalid was observed during the first 24 h, reaching approximately 40.5% and 55.5% inhibition of growth rate in UPW and LW, respectively. In contrast, significantly lower was the inhibition after exposure for 48 and 72 h. This phenomenon is correlated with the microalgal adaptation mechanism after exposure to toxic compounds [51]. This trend was also observed at the first stages of the process (30 and 60 min in UPW and 30, 60, 120, and 240 min in LW), where the toxicity levels increased, probably due to the formation of the identified TPs.

Based on the results obtained in Figure 5, the TPs were found to contribute to the overall toxicity, while probable synergistic effects between them can also be considered. The general tendency of pollutant mixtures to show synergistic effects due to their complexity compared to individual compounds is reported in the literature [52]. This was further

verified by the evaluation of the toxic response of boscalid in concentrations equal to those calculated during the photocatalytic process. As depicted in Figure S1, as the concentration of boscalid decreases, the toxic responses against the microalgae *Scenedesmus rubescens* also decline. However, with the prolonged application of heterogeneous photocatalysis the toxicity reduced significantly.

### *2.4. In silico Predicted Ecotoxicity and Toxicological Endpoints of Boscalid and Its TPs*

The potential effects of boscalid and its identified TPs were also evaluated using in silico tools, which required knowledge of the exact chemical structure of boscalid and its tentatively identified TPs to perform QSAR-based predictions. Of all the detected TPs, only the structure of TP_359 could not be fully elucidated, as the exact hydroxylation site could not be determined from the results of high-resolution mass spectrometry. Therefore, the four most probable hydroxylation sites of boscalid were taken into consideration and are presented in Figure S2, based on whether the functional groups of the A, B, and C rings were either ortho-, para-, or meta-directors, and the resulting structures were used by the in silico tools. However, all acute and chronic toxicity values, as well as other endpoints predicted by ECOSAR v2.2, T.E.S.T. v5.1.2, and Toxtree v2.6.13, for these four possible TP_359 structures showed little to no variation, and the results presented for TP_359 are averages to reflect more realistic data.

The acute and chronic toxicity values of boscalid and its TPs, which were assessed in silico for the three different aquatic trophic levels, are presented in Table S2. Although the software classified these compounds into more than one category, only the "Amides" classification was considered as it was the most common for the parent compound and its TPs (except for TP_325), and therefore the data could be more comparable.

The results generated by ECOSAR indicate that boscalid is a rather toxic compound for all three classes of aquatic organisms. These predicted data coincide with the findings of in vitro studies, which report that boscalid causes adverse effects in aquatic organisms such as *Daphnia magna* and *Danio rerio*, further supporting the fact that the presence of this fungicide could potentially pose a threat to aquatic ecosystems [25,53,54]. However, this is not the case for most of the tentatively identified TPs, because TP_307, TP_289, and TP_359, which were detected in both studied aqueous matrices (UPW and LW), are evaluated as less toxic than the parent compound. Interestingly, TP_325, along with TP_309, which was only detected when LW was utilized as a matrix, are the only TPs predicted to pose a greater ecotoxic threat than boscalid to fish, daphnids, and algae.

According to the bioconcentration factors presented in Figure 6a, the applied process generally led to the formation of compounds that are less likely to accumulate in living organisms, except for the very toxic TP_325, whose bioconcentration factor was found to be 4.5 times higher than boscalid, denoting that the overall ecotoxicological effect of this particular TP should be further investigated through in vitro approaches. The T.E.S.T estimations regarding developmental toxicity and mutagenicity (Figure 6b,c) indicate that photocatalysis with g-$C_3N_4$ does not limit these two toxicity-related problems significantly because, apart from TP_325, which was classified as a "developmental non-toxicant", all the other TPs were predicted as both "developmental toxicants" and "mutagenicity positive", with values similar or higher to those of boscalid. Therefore, from the results of both ECOSAR and T.E.S.T. it becomes evident that, for a greater detoxification effect, longer irradiation periods might be required. This agrees with the experimental ecotoxicity results presented in Section 2.3 using microalgae *Scenedesmus rubescens*, as the toxicity was increased at the first stages of the process; however, long-term application showed high detoxification.

Finally, the predictions of Toxtree, which are summarized in Table S3, do not show significant variations between boscalid and its TPs, apart from the fact that TP_325 was the only compound that could potentially induce genotoxicity related carcinogenesis.

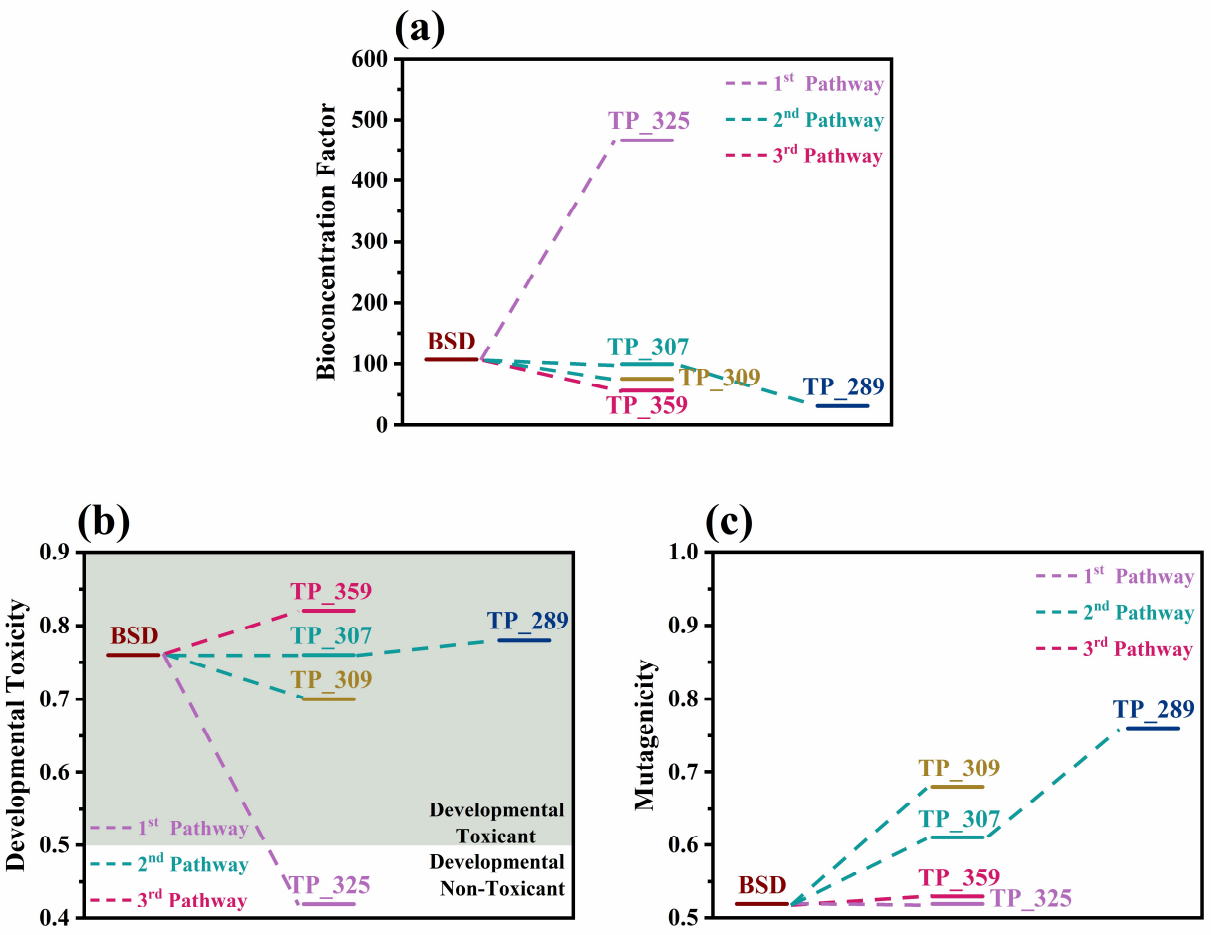


**Figure 6.** (**a**) Bioconcentration factors, (**b**) developmental toxicity, and (**c**) mutagenicity values of boscalid (BSD) and its TPs predicted by T.E.S.T. v5.1.2.

### *2.5. Reusability-Photocatalytic Cycles*

The reusability of the photocatalyst is a very important issue and is related to the catalyst's ability to remain active after its use. Thus, to evaluate the reusability of the g-$C_3N_4$ catalyst against the degradation of boscalid, experiments were conducted for five cycles (Figure 7), adopting the same experimental conditions. After each cycle, the catalyst was recovered, rinsed several times with ultrapure water, and dried at room temperature. It was observed that the efficiency of the g-$C_3N_4$ catalyst was nearly the same, even after three cycles using both UPW and LW, demonstrating that the g-$C_3N_4$ catalyst can be recovered and reused, retaining its photochemical stability and activity. The performance appeared to slightly decrease when it was repeated another two times. These results indicate that g-$C_3N_4$-based photocatalysis can be an alternative and sustainable option for the treatment of aqueous matrices contaminated with boscalid fungicide because it can reduce both operating and disposal costs by the reusability of the catalyst. Such recycling is in line with Green Chemistry principles, particularly concerning preventing waste.

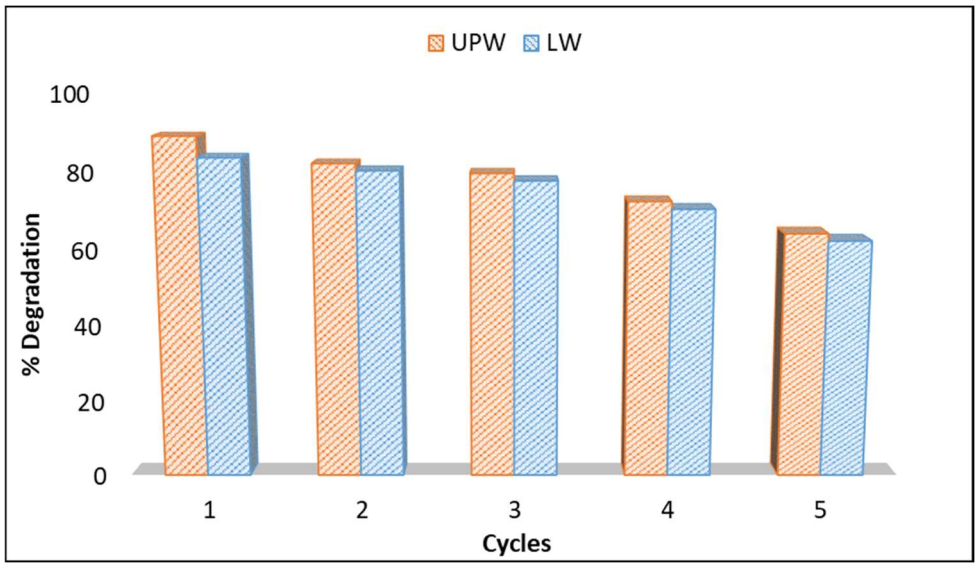


**Figure 7.** Reusability experiments of g-$C_3N_4$ catalyst.

## 3. Materials and Methods

### *3.1. Chemicals and Reagents*

Boscalid was obtained from Riedel de Haën. Graphitic carbon nitride (g-$C_3N_4$), with characteristics as depicted in Table 2, was used as the photocatalyst [34]. The synthesis and characterization of the photocatalyst is described elsewhere [34]. Acetonitrile, isopropanol, methanol, and water of HPLC-grade solvents were supplied by Merck. Formic acid and cyanobacteria BG-11 freshwater solution were purchased from Sigma-Aldrich (St. Louis, MO, USA). Ultrapure water and lake water (pH = 7.15 ± 0.02; total suspended solids = 2.17 ± 0.042 mg $L^{-1}$; total organic carbon = 11.6 ± 1.42 mg $L^{-1}$; $PO_4^{3-}$ = 4.05 ± 0.084 mg $L^{-1}$; $SO_4^{2-}$ = 22.1 ± 1.26 mg $L^{-1}$; $NO_3^-$ = 24.1 ± 0.78 mg $L^{-1}$) were used as matrices. Samples of the microalgae species *Scenedesmus rubescens* (strain SAG 5.95) were purchased from the bank SAG collection of Gottingen University (Germany).

**Table 2.** Surface area, particle size, and bandgap ($E_g$) of g-$C_3N_4$ catalyst [34].

| | Surface Area ($m^2$ $g^{-1}$) | Particle Size (nm) | $E_g$ (eV) |
|---|---|---|---|
| **g-$C_3N_4$** | 35 | 25 | 2.82 |

### *3.2. Photocatalytic Experiments*

Photocatalytic experiments were conducted using cylindrical pyrex glass cells with a total volume of 100 mL of aqueous solution containing the target compound in ultrapure water and lake water at a natural pH of 6.53–6.67 and 25 °C. Standard conditions were maintained across all experiments, with initial concentrations set at $[Boscalid]_0$ = 1 mg $L^{-1}$, $[g\text{-}C_3N_4]_0$ = 400 mg $L^{-1}$. The concentration of the catalysts was selected based on preliminary experiments, and the optimum concentration was found to be 400 mg $L^{-1}$. A relatively higher initial concentration of boscalid (1 mg $L^{-1}$) than the typical values found in surface waters has been selected in this study to obtain slower kinetics and provide favorable conditions for the identification and structural elucidation of the TPs.

UV-A illumination (315–400 nm) was administered using a custom-built "illumination box" equipped with four F15W/T8 black light tubes from Sylvania, emitting maximally at approximately 365 nm. Before the illumination, the boscalid solution containing g-$C_3N_4$ underwent a 30-min stirring period on a magnetic stirrer (Stuart SB 161-3, United Kingdom) in darkness to attain adsorption-desorption equilibrium. Sampling was carried out at specific intervals, with subsequent filtration using a Millex-GV PVDF 0.22 μm before further analysis.

The contribution of $HO^{\bullet}$ and $h^{+}$ to the degradation mechanism was evaluated using t-BuOH (0.1 mol $L^{-1}$) and KI (0.1 mol $L^{-1}$), respectively [42,55]. The role of superoxide anion radicals ($O_2^{\bullet -}$) was studied in an experiment conducted under $N_2$ atmosphere [55].

### *3.3. Analytical Methods*

HPLC and UHPLC/HRMS Analysis

The concentration of boscalid was quantified by a Dionex HPLC system. The identification of transformation products (TPs) was performed by UHPLC/HRMS. More details about HPLC and UHPLC/HRMS analysis are available in the Supplementary Materials (SM 1).

### *3.4. Algal Biotest*

Algal bioassays were conducted using *Scenedesmus rubescens* (strain SAG 5.95) according to OECD 201 protocol [56]. BG-11 was used as the culture medium, and sterile conditions and continuous illumination (4300 lux) were adopted. All the samples in concentrations of 5% $v/v$ were tested in triplicate and the inhibition (% I) growth rates were calculated. The results are expressed as the mean ± SD.

### *3.5. In Silico Toxicity Assessment Tools*

Predictions regarding the ecotoxicity of boscalid and its tentatively identified TPs as well as assessments of the important toxicological factors (e.g., mutagenicity) of these compounds were performed using three different publicly available in silico tools. In particular, the acute and chronic toxicity of the aforementioned compounds to three different categories (trophic levels) of aquatic organisms (i.e., fish, daphnid, and green algae) were assessed using the Ecological Structure Activity Relationships (ECOSAR) v2.2 software, which was developed by the United States Environmental Protection Agency (U.S. EPA) and utilizes quantitative structure–activity relationship (QSAR) models to make predictions [57]. Specifically, the software classifies chemical compounds based on their chemical structure and expresses acute toxicity values per organism category (after 96 h or 48 h of exposure) either as half-maximal effective concentration ($EC_{50}$) or half-maximal lethal concentration ($LC_{50}$), while chronic toxicity is expressed as chronic values (ChV). Depending on the predicted ChV, $LC_{50}$, and $EC_{50}$ values, boscalid and its TPs were also classified as either Very Toxic ($ChV/EC_{50}/LC_{50} \leq 1$ mg $L^{-1}$), Toxic (1 mg $L^{-1}$ < $ChV/EC_{50}/LC_{50} \leq 10$ mg $L^{-1}$), Harmful (10 mg $L^{-1}$ < $ChV/EC_{50}/LC_{50} \leq 100$ mg $L^{-1}$), or Not Harmful (100 mg $L^{-1}$ < $ChV/EC_{50}/LC_{50}$) to each category of the aforementioned aquatic organisms in accordance with the Globally Harmonized System of Classification and Labeling of Chemicals (GHS) [58]. The mutagenicity, developmental toxicity, and bioaccumulation factor (toxicological endpoints) of both boscalid and its TPs were predicted utilizing the Toxicity Estimation Software Tool (T.E.S.T.) v5.1.2, which, like ECOSAR, was also developed by the U.S. EPA and is based on using advanced QSAR methodologies to perform estimations [59]. In general, T.E.S.T. allows the application of five different QSAR methodologies; however, in this study all toxicological endpoints were predicted by the consensus method because, according to the software user's guide, it is the methodology that provides the most accurate results. The environmental persistence of the previously mentioned compounds as well as their oral toxicity and potential carcinogenicity were estimated by Toxtree v2.6.13 software, which was developed by Ideaconsult Ltd. (Sofia, Bulgaria) under a contract with the Joint Research Center (JRC) [60]. Toxtree is generally based on the application and the use of decision trees to perform predictions on various types of toxicological hazards (e.g., carcinogenicity) [61]. The results for each compound are presented as classifications according to the investigated hazard type. For example, in the case of environmental persistence the compounds are categorized as either Class 1 (easily biodegradable chemical), Class 2 (persistent chemical), or Class 3 (unknown biodegradability).

## 4. Conclusions

In the present study, the g-$C_3N_4$-based photocatalytic oxidation and detoxification of aqueous matrices (ultrapure water and lake water) contaminated with fungicide boscalid under UV-A irradiation was studied. The effectiveness of the process was evaluated using a holistic approach combining chemical methods, biological systems, and in silico study. The g-$C_3N_4$-based photocatalytic process was proved to effectively remove boscalid in both matrices, with a maximum efficiency exceeding 83%. However, a lower degradation rate was observed in LW ($k = 7.2 \times 10^{-3}$ $min^{-1}$ and $t_{1/2} = 96.3$ min), attributed to the complexity of this environmental matrix compared to ultrapure water. The assessment of ecotoxicity by exposing the microalgae *Scenedesmus rubescens* to boscalid before and after treatment was evaluated. UHPLC-HRMS analysis allowed the identification of five TPs, while the main degradation pathways involved hydroxylation, cyclization, and dechlorination. The identified TPs were in silico evaluated, and some of them were found to be toxic or very toxic for aquatic organisms. Moreover, some TPs were characterized as "developmental toxicants" and "mutagenicity positive" with values similar to those of boscalid or higher. The results from in silico study correlate with the observed evolution of ecotoxicity during the application of the process. Therefore, it becomes evident that, for a greater detoxification effect, longer application of the process is required. Finally, the studied g-$C_3N_4$ catalyst showed good reusability as it was found to retain almost the same photochemical activity for at least three cycles. Overall, this study indicates that the efficiency of water treatment processes needs detailed investigation using a wide range of experimental methods and computational approaches to provide data that can promote the large-scale applicability of a process without the generation of toxic by-products.

**Supplementary Materials:** The following supporting information can be downloaded at: https://www.mdpi.com/article/10.3390/catal14020112/s1, Table S1: LC-HRMS data for boscalid (BSD) and its TPs in UPW and LW by photocatalysis with g-$C_3N_4$; Table S2. Acute and chronic toxicity values of boscalid and its TPs predicted by ECOSAR v2.2; Table S3. Oral toxicity (Cramer rules), environmental persistence and carcinogenicity for boscalid and its TPs predicted by Toxtree v2.6.13; Figure S1: % Inhibition of growth rate of *Scenedesmus rubescens* after exposure to different concentrations of boscalid; Figure S2: Most probable hydroxylation sites for TP_359; SM 1. HPLC and UHPLC/HRMS analysis.

**Author Contributions:** Conceptualization, M.A. and I.K.; methodology, M.A., A.T., K.M., C.L. and I.K.; software, C.L.; validation, M.A. and I.K.; formal analysis, M.A., A.T., K.M., C.L. and I.K.; investigation, M.A., A.T., K.M., C.L. and I.K.; resources, M.A. and I.K.; data curation, M.A. and I.K.; writing—original draft, M.A., A.T., K.M., C.L. and I.K.; writing—review and editing, M.A. and I.K.; visualization, M.A., A.T., K.M., C.L. and I.K.; supervision, M.A. and I.K.; project administration, M.A.; funding acquisition, M.A. and I.K. All authors have read and agreed to the published version of the manuscript.

**Funding:** This research received no external funding.

**Data Availability Statement:** Data are contained within the article and Supplementary Materials.

**Acknowledgments:** The authors would like to thank the Unit of Environmental, Organic, and Biochemical high-resolution analysis–Orbitrap-LC–MS of the University of Ioannina, Greece for providing access to the facilities.

**Conflicts of Interest:** The authors declare no conflicts of interest.

## References

1. Dong, S.; Feng, J.; Fan, M.; Pi, Y.; Hu, L.; Han, X.; Liu, M.; Sun, J.; Sun, J. Recent Developments in Heterogeneous Photocatalytic Water Treatment Using Visible Light-Responsive Photocatalysts: A Review. *RSC Adv.* **2015**, *5*, 14610–14630. [CrossRef]
2. Dharma, H.N.C.; Jaafar, J.; Widiastuti, N.; Matsuyama, H.; Rajabsadeh, S.; Othman, M.H.D.; Rahman, M.A.; Jafri, N.N.M.; Suhaimin, N.S.; Nasir, A.M.; et al. A Review of Titanium Dioxide ($TiO_2$)-Based Photocatalyst for Oilfield-Produced Water Treatment. *Membranes* **2022**, *12*, 345. [CrossRef]
3. Wen, J.; Xie, J.; Chen, X.; Li, X. A Review on G-$C_3N_4$-Based Photocatalysts. *Appl. Surf. Sci.* **2017**, *391*, 72–123. [CrossRef]

4. Konstas, P.-S.; Kosma, C.; Konstantinou, I.; Albanis, T. Photocatalytic Treatment of Pharmaceuticals in Real Hospital Wastewaters for Effluent Quality Amelioration. *Water* **2019**, *11*, 2165. [CrossRef]
5. Moreira, N.F.F.; Sampaio, M.J.; Ribeiro, A.R.; Silva, C.G.; Faria, J.L.; Silva, A.M.T. Metal-Free g-$C_3N_4$ Photocatalysis of Organic Micropollutants in Urban Wastewater under Visible Light. *Appl. Catal. B Environ.* **2019**, *248*, 184–192. [CrossRef]
6. Zhao, G.-Q.; Zou, J.; Hu, J.; Long, X.; Jiao, F.-P. A Critical Review on Graphitic Carbon Nitride (g-$C_3N_4$)-Based Composites for Environmental Remediation. *Sep. Purif. Technol.* **2021**, *279*, 119769. [CrossRef]
7. Desen, Z.; Xuan, Z.; Zheng, L.; Jun, Z.; Tielin, W.; Shaowen, C. Construction of local coordination environment of iron sites over g-$C_3N_4$/PCN-222 (Fe) composite with high $CO_2$ photoreduction performance. *Appl. Catal. B Environ.* **2024**, *334*, 123639. [CrossRef]
8. Jia, J.; Luo, Y.; Wu, H.; Wang, Y.; Jia, X.; Wan, J.; Dang, Y.; Liu, G.; Xie, H.; Zhang, Y. Nickel selenide/g-$C_3N_4$ heterojunction photocatalyst promotes C-C coupling for photocatalytic $CO_2$ reduction to ethane. *J. Colloid Interface Sci.* **2024**, *658*, 966–975. [CrossRef]
9. Abdullah, B.; Nor, A.S.A.; Aniz, C.U.; Shakeel, A.; Ahmed, T.A.-Q.; Jamilu, U.; Nagendra, K.; Gazali, T. Well-designed glucose precursor carbon/g-$C_3N_4$ nanocomposite for enhanced visible light photocatalytic $CO_2$ reduction activity. *J. Photochem. Photobiol. A Chem.* **2024**, *447*, 115272. [CrossRef]
10. Yang, Z.; Tang, P.; Xu, C.; Zhu, B.; He, Y.; Duan, T.; He, J.; Zhang, G.; Cui, P. Graphitic carbon nitride (g-$C_3N_4$) as a super support for Mn-Ce based $NH_3$-SCR catalyst: Improvement of catalytic performance and $H_2O/SO_2$ tolerance for $NO_x$ removal. *J. Energy Inst.* **2023**, *108*, 101201. [CrossRef]
11. Qi, K.; Jing, J.; Dong, G.; Li, P.; Huang, Y. The excellent photocatalytic NO removal performance relates to the synergistic effect between the prepositive NaOH solution and the g-$C_3N_4$ photocatalysis. *Environ. Res.* **2022**, *212*, 113405. [CrossRef]
12. Yu, C.; Yang, H.; Zhao, H.; Huang, X.; Liu, M.; Du, C.; Chen, R.; Feng, J.; Dong, S.; Sun, J.; et al. Simultaneous hydrogen production from wastewater degradation by protonated porous g-$C_3N_4$/$BiVO_4$ Z-scheme composite photocatalyst. *Sep. Purif. Technol.* **2024**, *335*, 126201. [CrossRef]
13. Ni, F.; Zhang, A.; Lu, H.; Weng, B.; Zhang, Q.; Li, H.; Zheng, H.; Pang, S. Investigation into performance of $Ag_2O$/g-$C_3N_4$ p-n heterojunction photocatalysts with efficient $H_2$ production activity. *J. Solid State Chem.* **2024**, *330*, 124449. [CrossRef]
14. Alaghmandfard, A.; Ghandi, K. A Comprehensive Review of Graphitic Carbon Nitride (g-$C_3N_4$)–Metal Oxide-Based Nanocomposites: Potential for Photocatalysis and Sensing. *Nanomaterials* **2022**, *12*, 294. [CrossRef]
15. Liu, X.; Ma, R.; Zhuang, L.; Hu, B.; Chen, J.; Liu, X.; Wang, X. Recent Developments of Doped g-$C_3N_4$ Photocatalysts for the Degradation of Organic Pollutants. *Crit. Rev. Environ. Sci. Technol.* **2021**, *51*, 751–790. [CrossRef]
16. Ahmad, A.; Tariq, S.; Zaman, J.U.; Martin Perales, A.I.; Mubashir, M.; Luque, R. Recent Trends and Challenges with the Synthesis of Membranes: Industrial Opportunities towards Environmental Remediation. *Chemosphere* **2022**, *306*, 135634. [CrossRef] [PubMed]
17. Münze, R.; Hannemann, C.; Orlinskiy, P.; Gunold, R.; Paschke, A.; Foit, K.; Becker, J.; Kaske, O.; Paulsson, E.; Peterson, M.; et al. Pesticides from Wastewater Treatment Plant Effluents Affect Invertebrate Communities. *Sci. Total Environ.* **2017**, *599–600*, 387–399. [CrossRef] [PubMed]
18. Reilly, T.J.; Smalling, K.L.; Orlando, J.L.; Kuivila, K.M. Occurrence of Boscalid and Other Selected Fungicides in Surface Water and Groundwater in Three Targeted Use Areas in the United States. *Chemosphere* **2012**, *89*, 228–234. [CrossRef] [PubMed]
19. Karlsson, A.S.; Weihermüller, L.; Tappe, W.; Mukherjee, S.; Spielvogel, S. Field Scale Boscalid Residues and Dissipation Half-Life Estimation in a Sandy Soil. *Chemosphere* **2016**, *145*, 163–173. [CrossRef] [PubMed]
20. Hatzilazarou, S.P.; Charizopoulos, E.T.; Papadopoulou-Mourkidou, E.; Economou, A.S. Dissipation of Three Organochlorine and Four Pyrethroid Pesticides Sprayed in a Greenhouse Environment during Hydroponic Cultivation of Gerbera. *Pest Manag. Sci.* **2004**, *60*, 1197–1204. [CrossRef] [PubMed]
21. Smalling, K.L.; Orlando, J.L. *Occurrence of Pesticides in Surface Water and Sediments from Three Central California Coastal Watersheds, 2008–2009*; U.S. Geological Survey Data Series 600: Reston, VA, USA, 2011. [CrossRef]
22. Smalling, K.L.; Reilly, T.J.; Sandstrom, M.W.; Kuivila, K.M. Occurrence and Persistence of Fungicides in Bed Sediments and Suspended Solids from Three Targeted Use Areas in the United States. *Sci. Total Environ.* **2013**, *447*, 179–185. [CrossRef]
23. Qian, L.; Cui, F.; Yang, Y.; Liu, Y.; Qi, S.; Wang, C. Mechanisms of Developmental Toxicity in Zebrafish Embryos (Danio Rerio) Induced by Boscalid. *Sci. Total Environ.* **2018**, *634*, 478–487. [CrossRef]
24. Aksakal, F.I. Evaluation of Boscalid Toxicity on Daphnia Magna by Using Antioxidant Enzyme Activities, the Expression of Genes Related to Antioxidant and Detoxification Systems, and Life-History Parameters. *Comp. Biochem. Physiol. C Toxicol. Pharmacol.* **2020**, *237*, 108830. [CrossRef] [PubMed]
25. Qian, L.; Qi, S.; Cao, F.; Zhang, J.; Zhao, F.; Li, C.; Wang, C. Toxic Effects of Boscalid on the Growth, Photosynthesis, Antioxidant System and Metabolism of Chlorella Vulgaris. *Environ. Pollut.* **2018**, *242*, 171–181. [CrossRef]
26. Lebrun, J.D.; De Jesus, K.; Tournebize, J. Individual Performances and Biochemical Pathways as Altered by Field-Realistic Exposures of Current-Use Fungicides and Their Mixtures in a Non-Target Species, Gammarus Fossarum. *Chemosphere* **2021**, *277*, 130277. [CrossRef] [PubMed]
27. Aliste, M.; Pérez-Lucas, G.; Vela, N.; Garrido, I.; Fenoll, J.; Navarro, S. Solar-Driven Photocatalytic Treatment as Sustainable Strategy to Remove Pesticide Residues from Leaching Water. *Environ. Sci. Pollut. Res.* **2020**, *27*, 7222–7233. [CrossRef] [PubMed]

28. Aliste, M.; Garrido, I.; Pérez-Lucas, G.; Flores, P.; Hellín, P.; Navarro, S.; Fenoll, J. Appraisal of Water Matrix on the Removal of Fungicide Residues by Heterogeneous Photocatalytic Treatment Using UV-LED Lamp as Light Source. *Environ. Sci. Pollut. Res.* **2021**, *28*, 23849–23858. [CrossRef]
29. Aznar-Cervantes, S.; Aliste, M.; Garrido, I.; Yañez-Gascón, M.J.; Vela, N.; Cenis, J.L.; Navarro, S.; Fenoll, J. Electrospun Silk Fibroin/$TiO_2$ Mats. Preparation, Characterization and Efficiency for the Photocatalytic Solar Treatment of Pesticide Polluted Water. *RSC Adv.* **2020**, *10*, 1917–1924. [CrossRef]
30. Choi, S.W.; Shahbaz, H.M.; Kim, J.U.; Kim, D.-H.; Yoon, S.; Jeong, S.H.; Park, J.; Lee, D.-U. Photolysis and $TiO_2$ Photocatalytic Treatment under UVC/VUV Irradiation for Simultaneous Degradation of Pesticides and Microorganisms. *Appl. Sci.* **2020**, *10*, 4493. [CrossRef]
31. Lagunas-Allué, L.; Martínez-Soria, M.-T.; Sanz-Asensio, J.; Salvador, A.; Ferronato, C.; Chovelon, J.M. Photocatalytic Degradation of Boscalid in Aqueous Titanium Dioxide Suspension: Identification of Intermediates and Degradation Pathways. *Appl. Catal. B Environ.* **2010**, *98*, 122–131. [CrossRef]
32. Taha, S.M.; Amer, M.E.; Elmarsafy, A.M.; Elkady, M.Y.; Chovelon, J.-M. Degradation of Boscalid by Nitrogen-Doped/Undoped $TiO_2$ and Persulfate Ions Using Different Activation Conditions and the Identification of Its Main Degradation Products Using LC/MS/MS. *Chem. Eng. J.* **2016**, *288*, 845–857. [CrossRef]
33. Liu, X.; Yu, W.; Li, C.; Zhang, B.; Yun, M.; Ma, Y. Impact of Unadorned Carbon Nitride on Photodegradation and Bioavailability of Multifungicides in the Environment. *J. Agric. Food Chem.* **2021**, *69*, 28–35. [CrossRef]
34. Konstas, P.-S.; Konstantinou, I.; Petrakis, D.; Albanis, T. Synthesis, Characterization of g-$C_3N_4$/$SrTiO_3$ Heterojunctions and Photocatalytic Activity for Organic Pollutants Degradation. *Catalysts* **2018**, *8*, 554. [CrossRef]
35. Antonopoulou, M.; Bika, P.; Papailias, I.; Zervou, S.-K.; Vrettou, A.; Efthimiou, I.; Mitrikas, G.; Ioannidis, N.; Trapalis, C.; Dallas, P.; et al. Photocatalytic Degradation of Organic Micropollutants under UV-A and Visible Light Irradiation by Exfoliated g-$C_3N_4$ Catalysts. *Sci. Total Environ.* **2023**, *892*, 164218. [CrossRef]
36. Bairamis, F.; Konstantinou, I.; Petrakis, D.; Vaimakis, T. Enhanced Performance of Electrospun Nanofibrous $TiO_2$/g-$C_3N_4$ Photocatalyst in Photocatalytic Degradation of Methylene Blue. *Catalysts* **2019**, *9*, 880. [CrossRef]
37. Liu, X.; Zong, H.; Tan, X.; Wang, X.; Qiu, J.; Kong, F.; Zhang, J.; Fang, S. Facile synthesis of modified carbon nitride with en-hanced activity for photocatalytic degradation of atrazine. *J. Environ. Chem. Eng.* **2021**, *9*, 105807. [CrossRef]
38. Altendji, K.; Hamoudi, S. Efficient Photocatalytic Degradation of Aqueous Atrazine over Graphene-Promoted g-$C_3N_4$ Nanosheets. *Catalysts* **2023**, *13*, 1265. [CrossRef]
39. Ioannidou, E.; Frontistis, Z.; Antonopoulou, M.; Venieri, D.; Konstantinou, I.; Kondarides, D.I.; Mantzavinos, D. Solar Photocatalytic Degradation of Sulfamethoxazole over Tungsten—Modified $TiO_2$. *Chem. Eng. J.* **2017**, *318*, 143–152. [CrossRef]
40. Spyrou, A.; Tzamaria, A.; Dormousoglou, M.; Skourti, A.; Vlastos, D.; Papadaki, M.; Antonopoulou, M. The Overall Assessment of Simultaneous Photocatalytic Degradation of Cimetidine and Amisulpride by Using Chemical and Genotoxicological Approaches. *Sci. Total Environ.* **2022**, *838*, 156140. [CrossRef] [PubMed]
41. Calza, P.; Hadjicostas, C.; Sakkas, V.A.; Sarro, M.; Minero, C.; Medana, C.; Albanis, T.A. Photocatalytic Transformation of the Antipsychotic Drug Risperidone in Aqueous Media on Reduced Graphene Oxide—$TiO_2$ Composites. *Appl. Catal. B Environ.* **2016**, *183*, 96–106. [CrossRef]
42. Liang, C.; Su, H.-W. Identification of Sulfate and Hydroxyl Radicals in Thermally Activated Persulfate. *Ind. Eng. Chem. Res.* **2009**, *48*, 5558–5562. [CrossRef]
43. Antonopoulou, M.; Papadaki, M.; Rapti, I.; Konstantinou, I. Photocatalytic Degradation of Pharmaceutical Amisulpride Using g-$C_3N_4$ Catalyst and UV-A Irradiation. *Catalysts* **2023**, *13*, 226. [CrossRef]
44. Bhatt, D.; Srivastava, A.; Srivastava, P.C.; Sharma, A. Evaluation of Three Novel Soil Bacterial Strains for Efficient Biodegradation of Persistent Boscalid Fungicide: Kinetics and Identification of Microbial Biodegradation Intermediates. *Environ. Pollut.* **2023**, *316*, 120484. [CrossRef] [PubMed]
45. Skanes, B.; Warriner, K.; Prosser, R.S. Hazard Assessment Using an In-Silico Toxicity Assessment of the Transformation Products of Boscalid, Pyraclostrobin, Fenbuconazole and Glyphosate Generated by Exposure to an Advanced Oxidative Process. *Toxicol. In Vitro* **2021**, *70*, 105049. [CrossRef] [PubMed]
46. Lassalle, Y.; Kinani, A.; Rifai, A.; Souissi, Y.; Clavaguera, C.; Bourcier, S.; Jaber, F.; Bouchonnet, S. UV-Visible Degradation of Boscalid—Structural Characterization of Photoproducts and Potential Toxicity Using in Silico Tests. *Rapid Commun. Mass Spectrom.* **2014**, *28*, 1153–1163. [CrossRef] [PubMed]
47. Jabot, C.; Daniele, G.; Giroud, B.; Tchamitchian, S.; Belzunces, L.P.; Casabianca, H.; Vulliet, E. Detection and Quantification of Boscalid and Its Metabolites in Honeybees. *Chemosphere* **2016**, *156*, 245–251. [CrossRef]
48. Mojiri, A.; Nazari Vishkaei, M.; Ansari, H.K.; Vakili, M.; Farraji, H.; Kasmuri, N. Toxicity Effects of Perfluorooctanoic Acid (PFOA) and Perfluorooctane Sulfonate (PFOS) on Two Green Microalgae Species. *Int. J. Mol. Sci.* **2023**, *24*, 2446. [CrossRef]
49. Kalamaras, G.; Kloukinioti, M.; Antonopoulou, M.; Ntaikou, I.; Vlastos, D.; Eleftherianos, A.; Dailianis, S. The Potential Risk of Electronic Waste Disposal into Aquatic Media: The Case of Personal Computer Motherboards. *Toxics* **2021**, *9*, 166. [CrossRef]
50. Antonopoulou, M.; Dormousoglou, M.; Spyrou, A.; Dimitroulia, A.A.; Vlastos, D. An Overall Assessment of the Effects of Antidepressant Paroxetine on Aquatic Organisms and Human Cells. *Sci. Total Environ.* **2022**, *852*, 158393. [CrossRef]
51. Babiak, W.; Krzemińska, I. Extracellular Polymeric Substances (EPS) as Microalgal Bioproducts: A Review of Factors Affecting EPS Synthesis and Application in Flocculation Processes. *Energies* **2021**, *14*, 4007. [CrossRef]

52. Rosal, R.; Rodea-Palomares, I.; Boltes, K.; Fernández-Piñas, F.; Leganés, F.; Petre, A. Ecotoxicological Assessment of Surfactants in the Aquatic Environment: Combined Toxicity of Docusate Sodium with Chlorinated Pollutants. *Chemosphere* **2010**, *81*, 288–293. [CrossRef] [PubMed]
53. Qian, L.; Qi, S.; Zhang, J.; Duan, M.; Schlenk, D.; Jiang, J.; Wang, C. Exposure to Boscalid Induces Reproductive Toxicity of Zebrafish by Gender-Specific Alterations in Steroidogenesis. *Environ. Sci. Technol.* **2020**, *54*, 14275–14287. [CrossRef]
54. Qian, L.; Qi, S.; Wang, Z.; Magnuson, J.T.; Volz, D.C.; Schlenk, D.; Jiang, J.; Wang, C. Environmentally Relevant Concentrations of Boscalid Exposure Affects the Neurobehavioral Response of Zebrafish by Disrupting Visual and Nervous Systems. *J. Hazard. Mater.* **2021**, *404*, 124083. [CrossRef] [PubMed]
55. Palominos, R.; Freer, J.; Mondaca, M.A.; Mansilla, H.D. Evidence for Hole Participation during the Photocatalytic Oxidation of the Antibiotic Flumequine. *J. Photochem. Photobiol. A* **2008**, *193*, 139–145. [CrossRef]
56. OECD. *Test No. 201: Freshwater Alga and Cyanobacteria, Growth Inhibition Test*; Organisation for Economic Co-Operation and Development: Paris, France, 2011.
57. USEPA. Ecological Structure Activity Relationships (ECOSAR) Predictive Model. Available online: https://www.epa.gov/tsca-screening-tools/ecological-structure-activity-relationships-ecosar-predictive-model (accessed on 25 December 2023).
58. Globally Harmonized System of Classification and Labelling of Chemicals (GHS Rev. 9, 2021) | UNECE. Available online: https://unece.org/transport/standards/transport/dangerous-goods/ghs-rev9-2021 (accessed on 25 December 2023).
59. USEPA. Toxicity Estimation Software Tool (TEST). Available online: https://www.epa.gov/comptox-tools/toxicity-estimation-software-tool-test (accessed on 25 December 2023).
60. Institute for Health and Consumer Protection (Joint Research Centre); Benigni, R.; Tcheremenskaia, O. *Computational Characterisation of Chemicals and Datasets in Terms of Organic Functional Groups—A New Toxtree Rulebase*; Publications Office of the European Union: Luxembourg, 2011.
61. Pavan, M.; Worth, A.P. Publicly-Accessible QSAR Software Tools Developed by the Joint Research Centre. *SAR QSAR Environ. Res.* **2008**, *19*, 785–799. [CrossRef] [PubMed]